Efficiency Improvement and Power Loss Breakdown for a Lundell-Alternator/Active-Rectifier System in Automotive Applications

Dimitrios Sarafianos*
Timothy J. Flack
Electrical Engineering Department
University of Cambridge
Cambridge, CB3 0FA, UK
Email: d.n.sarafianos@gmail.com

Danilo X Llano†
Richard A McMahon
WMG
University of Warwick
Coventry, CV4 7AL, UK
Email: dxl20@cantab.net

Bo Wen
School of Electrical and
Electronic Engineering
University of Manchester
Manchester, M13 9PL, UK

Stephen Pickering
JaguarLandRover Ltd.
Coventry, UK

***Abstract*—A control strategy for a conventional Lundell alternator and an active-rectifier using different modulation schemes was proposed in previous work. The modulation techniques examined indicated that the system could operate more efficiently than a passive rectifier over a certain speed and power range. This paper extends the modulation scheme analysis using a SVM scheme with six commutations per switching cycle, giving better electrical and overall efficiency. Furthermore, a power loss breakdown is performed for the active-rectifier with the assistance of experimental and simulation results of double pulse tests. Switching loss estimation curves are produced allowing the loss examination of the active-rectifier. Switching losses account only for a minor portion of the total rectifier losses in comparison to conduction losses. Finally, a higher dc-link voltage of 14.5 V was introduced using SVM scheme, giving better efficiency, in order to exploit further the rectifier loss distribution.**

***Index Terms*—Lundell alternator, active-rectifier, automotive, switching losses, conduction losses.**

I. Introduction

Although fully electric and other low emission vehicles are already been rolled out, future trends indicate that even at the best case scenario, gasoline and diesel will still play an important role in the light duty vehicles sector, which is greater than 50% by 2050 [1]. As a result, conventional vehicles are expected to be produced in the short and mid term future utilising Lundell alternators that will be used in the majority of the automotive fleet for a number of reasons, such as cost, robustness and speed-range [2].

There is limited literature on combining an active-rectifier with a Lundell alternator instead of the conventional PN Zener diode passive rectifier [3]–[7]. The majority of these studies consider synchronous rectification schemes [3]–[6]. The active-rectifier strategy used in [7] is not described, while the use of IGBTs as the rectifier topology for this low dc voltage application and its subsequent high-forward voltage drop compromises the rectifier efficiency.

This work was financially supported by JaguarLandRover Ltd.

The efficiency improvement of the electric power generation system of a conventional vehicle was investigated by connecting a Lundell alternator to an active-rectifier [8]. The control references were calculated using a cost-function and a control scheme was implemented in order to control the dq current values of the alternator's phase current. So, the alternator can be operated at its optimum operating points. There is a number of challenges to be resolved in the implementation of an active-rectifier control scheme in a Lundell alternator constructed for use with a passive rectifier. First, its high stator inductance value in conjunction with the high number of pole pairs (12 to 18) and speed range (up to 18,000 rpm) results in a high inductive reactance [2]. Furthermore, the low voltage bus requires a significant amount of dc current to supply the loads (up to 100 A). This will result in a significant voltage drop at the stator winding, alongside the need of a reactive current component to keep the dc bus voltage within limits. Therefore, the ratio between the active and reactive current components will ultimately set the compromise on the system efficiency. Third, the existence of the field winding suggests the existence of one additional degree of freedom, which complicates the implementation of the control strategy of the alternator/active-rectifier system. Sarafianos *et al.* presented in [9] a control strategy that addresses the challenges of active rectification. In this present paper a new Space Vector Modulation (SVM) is introduced with six commutations per switching cycle and the results are compared to the modulated schemes found in [9].

Few papers have focused on 14 V conventional vehicle power system using active rectification and associated losses. Similarly, most of the literature on losses and efficiency in power conversion is concentrated on applications with medium and high voltage (> 50 V) where the share between switching and conduction losses is fairly equal [10]–[12]. The aim of this work is also to investigate the active-rectifier losses and to quantify them into switching and conduction losses in a low voltage, high current application. The comparison of different active-rectifier modulation schemes allowed the identification

of the best performing scheme in terms of its electrical efficiency. This efficiency reflects the power losses between the ac generated power and the dc output power of every scheme. These losses include the conduction and switching losses of the active-rectifier and they depend on a number of electrical parameters, for example those arising from the PCB design. As a result, device characterisation information from manufacturer datasheets alone cannot be used. For this reason, a method for estimating the switching losses during turn-on and turn-off transients for the MOSFETs in their PCB was explored. Switching power losses and power measurements allowed the extraction of rectifier conduction losses. A double pulse test simulation study was carried out to estimate the switching losses based on an ideal case with no parasitic inductances and a second case where the estimated stray inductance was included in the simulation. The switching losses prediction curves are produced. These curves together with the power measurements assisted in extracting the rectifier conduction losses. Finally, the study has been extended to investigate the benefits of a 14.5 V dc-link. The higher dc-link voltage permitted significantly better efficiencies but its maximum value is limited by automotive industry standards and regulations.

II. Active-rectifier for automotive applications

A. Experimental setup

The experimental setup used to measure the efficiency of the Lundell alternator/ active-rectifier system is presented in Fig. 1. The alternator is the Bosch LiX 180 A, 2.4 kW with a three-phase delta-connected stator winding.

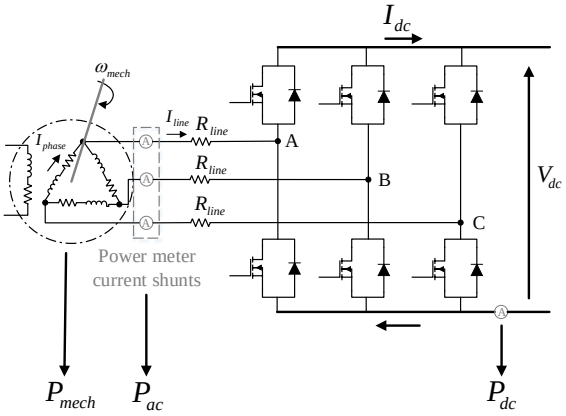

Figure 1: Experimental setup diagram

The measuring system has the connection between the current shunts, that measure the line current, and the active-rectifier's PCB, which consists of a number of connectors and 16 mm^2 tri-rated cables in order to handle the high current values of the application. As a result, an additional resistance (R_{line}) is present, as depicted at the schematic in Fig. 1. This resistance (R_{line}) compromises the power capability of the alternator by acting as an additional output impedance as well as introducing conduction losses. The resistance of the cables and connectors was measured for all three phases using a four-wire terminal ohmmeter and the average value was found to be 3.5 $m\Omega$. This unavoidable parasitic resistance value is significant, considering that is of the same magnitude than the on-resistance (R_{DSon} = 2.8 $m\Omega$) of a single rectifier's MOSFET and the resistance of the PCB tracks.

B. Efficiency measurements

An SVM scheme featuring six commutations per switching cycle is introduced in this paper and is compared against the modulation schemes presented by Sarafianos *et al.* in [9] in an effort to improve the overall system efficiency by decreasing the switching losses. The SVM scheme has six commutations per switching cycle, which are reduced by 50% compared to the 12 commutations in the third harmonic modulation scheme and 25% compared to the 8 commutations in the DSVM scheme. Fig. 11 in Appendix illustrates the efficiency compared to the results in [9] at different speed points. The passive rectifier results and the sinusoidal PWM (sPWM) are given only as a reference. The use of the SVM scheme improves both the electrical ($\frac{P_{dc}}{P_{ac}}$) and the overall system ($\frac{P_{dc}}{P_{mech}}$) efficiency.

C. Current waveforms and harmonics distortion

The smaller number of commutations in the SVM modulation increases the ripple of the current waveform. Fig. 2 depicts the current waveforms for the three different modulation schemes and their corresponding THD. It can be seen that in all cases the current is essentially sinusoidal with low THD, which is mainly due to the large filtering effect of the alternator's line inductance, especially at higher speeds.

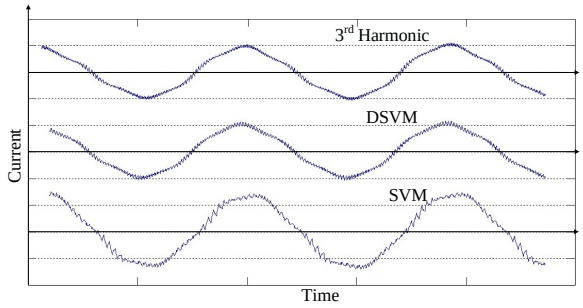

Figure 2: Current waveforms for different modulation schemes at 2000 rpm and 180 W. 3rd harmonic (THD=6.4%), DSVM (THD=6.7%) and SVM (THD=6.8%)

III. Double pulse test

The results in the previous section showed the effect of changing the number of commutations in the electrical efficiency of the rectifier but there is still a need to quantify the actual switching losses, establish their share on the total losses figure and explore opportunities for further loss reduction. The double pulse test allows the estimation of switching losses, which depend on the voltage, the current, the switching

frequency, the semiconductor device turn-on and turn-off times and the PCB layout [13]. The design of the PCB is of crucial importance to switching losses because it might introduce stray inductance that increases these losses [13]. The results of the double pulse test give the switching energy loss during the turn-on and turn-off transient of a single MOSFET including the aforementioned dependencies in this practical experiment.

A. Circuit setup and inductance measurement

The scheme of one leg of the active-rectifier is illustrated in Fig. 3, where the driver circuit (AUIR2113S) and the low-side MOSFET switch (IPP120N08S4-03) are included. Instead of a high-side switch, a SiC diode was placed (SiC_{diode}) in parallel to an inductor (L). A SiC diode (STPSC20H065C-Y) is used because it has no reverse recovery, thus no additional losses are added [13]. The resulted circuit was connected to ceramic capacitors (C_{cer}), which were mounted very close to minimise stray inductance and absorb transients, and to bulk electrolytic capacitors (C_{elect}) to store the required energy, during the off-time, and keep the dc-link voltage (V_{dc}) at the required level. Finally, the dc-link voltage was set to 14 V by a dc power supply. The stray inductance of the PCB under test was measured with an impedance meter (BK891 LCR Meter). Test conditions were chosen so that the measurements are within 5% accuracy according to the equipment specifications. The source to ground inductance was measured to be around 5.4 nH and the load to drain inductance was 8.5 nH giving a total stray inductance of about 14 nH. It should be noted that the inductance related to the MOSFET package itself (TO-220) is around 5 nH [14].

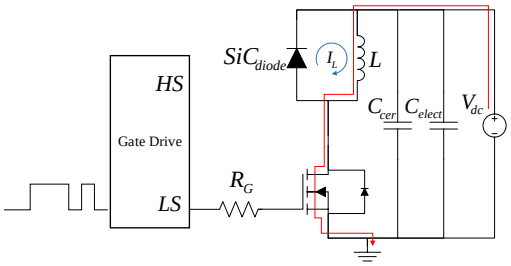

Figure 3: Double pulse circuitry

B. Switching losses curves

LTSpice simulations of the double pulse test were carried out to estimate the switching losses in two different scenarios. The first set of simulations considered an ideal circuit and PCB without any parasitic inductances. The second set of simulations included the measured inductances to mimic the actual PCB as realistically as possible. The simulation file was based on the scheme shown in Fig. 3 and the Spice models provided by the manufacturers of the diodes, MOSFET and gate driver. Fig. 4 displays the double pulse waveforms for 50 A current. The effects of the dc-link stray inductance can be clearly seen in the Vds waveform.

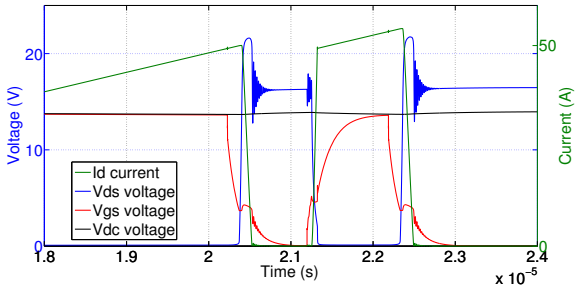

Figure 4: Double pulse waveforms

The double pulse test estimates the turn-on (E_{losses}^{ON}) and turn-off (E_{losses}^{OFF}) energy losses. The power losses in one complete switching event (turn-on and off) are calculated as:

$$P_{losses}^{switch} = \left(E_{losses}^{ON} + E_{losses}^{OFF}\right) \times f_{switching} \quad (1)$$

Fig. 5 shows the power losses for the ideal circuit and the circuit with parasitics at a switching frequency ($f_{switching}$) of 20 kHz. The stray inductance in the circuit significantly increases the losses.

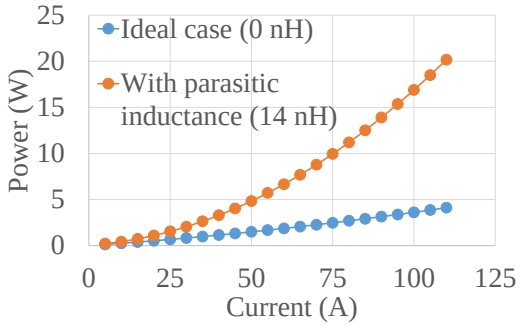

Figure 5: Device switching losses at 20 kHz

IV. Electrical Power Loss Breakdown

Only the SVM modulation is considered for further study as it has the best performance, but the process in this section could be extended to other modulation schemes. Having already measured the ac generated power (P_{ac}) and the dc output power (P_{dc}) for the different modulation schemes at different speed and power levels (Fig. 11), the power losses between these two points are divided into the following components:

$$P_{AC}^{losses} = P_{line} + P_{cond}^{rect} + P_{switc}^{rect} \quad (2)$$

where P_{AC}^{losses} are the losses between the power meter current shunts and the dc-link, P_{line} are the losses at the cables/connectors between the current shunts and the connectors to the active-rectifier (A, B and C points in Fig. 1), P_{cond}^{rect} are the conduction losses of the active-rectifier and P_{switc}^{rect} are the switching losses of the active-rectifier. The

ac current waveform of the active-rectifier has low THD as already presented in subsection II-C, with the highest value of 7% at light load and at the lowest speed. Therefore, the current can be considered sinusoidal and the line resistance power loss is calculated from $P_{line} = I_{line}^2 R_{line}$, where I_{line} is the ac rms line current. The result of the calculation is then subtracted from the values of the ac power reported in II-B. The remaining losses comprise the conduction and switching losses of the active-rectifier.

A. Rectifier loss breakdown for the SVM scheme

The rectifier loss breakdown using the switching losses estimated in section III for both, the ideal model and the actual circuit with parasitic inductances is depicted in Fig. 6. It is evident that conduction losses are significantly higher than the switching losses.

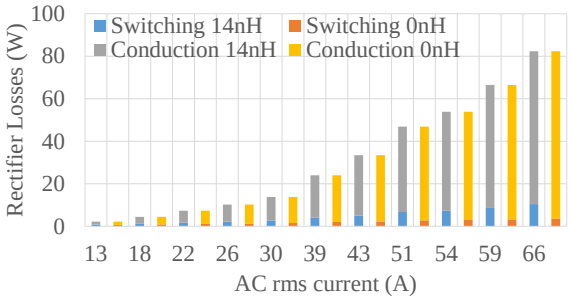

Figure 6: Rectifier loss breakdown for 2000 rpm

The conduction losses were estimated for different speeds and power points (currents) as shown in Fig. 7. There is a clear quadratic trend regardless of the operating speed, but these losses are higher than the values calculated with $I^2 R_{DSon}$, where R_{DSon} is the MOSFET on-resistance, 2.8 mΩ.

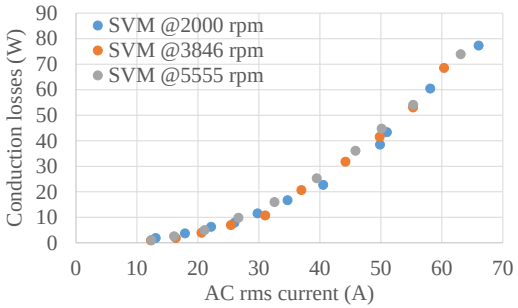

Figure 7: Rectifier conduction losses at different speeds

B. Conduction losses - analytical approach

The rectifier conduction losses are divided into MOSFET and diode conduction losses. The following equations can be used for the calculation of these losses once all the parameters are known [15]:

$$P_{MOSFET}^{cond} = R_{DSon} I_0^2 \left(\frac{1}{8} + \frac{m_a \cos\varphi}{3\pi} \right) \quad (3)$$

$$P_{DIODE}^{cond} = R_D I_0^2 \left(\frac{1}{8} - \frac{m_a \cos\varphi}{3\pi} \right) + u_D I_0 \left(\frac{1}{2\pi} - \frac{m_a \cos\varphi}{8} \right) \quad (4)$$

where, P_{MOSFET}^{cond} are MOSFET conduction losses, P_{DIODE}^{cond} are diode conduction losses. R_{DSon} is the MOSFET on-resistance, I_0 is the peak value of the ac line current, m_a is the modulation index (set to 0.925 in the controller), φ the angle between the line current and voltage, R_D is the equivalent diode resistance extracted from the MOSFET datasheet and u_D is the diode's forward voltage drop. The overall equation of the rectifier conduction losses is:

$$P_{total} = I_0^2 \left[R_{DSon} \left(\frac{1}{8} + \frac{m_a \cos\varphi}{3\pi} \right) + R_D \left(\frac{1}{8} - \frac{m_a \cos\varphi}{3\pi} \right) \right] - I_0 \left[u_D \left(\frac{1}{2\pi} - \frac{m_a \cos\varphi}{8} \right) \right] \quad (5)$$

The rectifier conduction losses depend on a number of non-constant factors as seen in Eq. (5) [15], [16]. However, the calculation becomes more complicated considering the dependency on temperature, because of the on-resistance of the MOSFET, the forward voltage drop, and the equivalent resistance of the diode as well as the amount of ac current flowing through each component with respect to the ac voltage (power factor, stray inductance, inductive load). Fig. 8 illustrates the schematic of one leg of the converter considering rectifier operation and assists in the selection of adequate signs for Eq. (5).

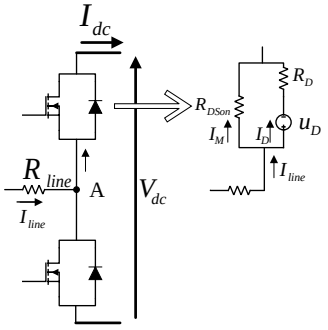

Figure 8: Conduction losses - Single leg diagram

C. Discussion of results

The loss breakdown shows that the switching losses account for less than 12.5% of the total rectifier losses in applications with low dc-link voltage (14 V) and high current. This distribution of losses is significantly different from the one observed in applications with a higher dc-link voltage, where the switching losses are around 50% of the total rectifier losses [17]. Therefore, any effort on reducing the switching losses by means such as a better PCB layout or lead-less packages for the MOSFETs (package inductance lower than 1 nH [14]) is valuable, but it will not have a significant impact

on the rectifier and overall efficiency. On the other hand, the conduction losses depend on the current going through the MOSFET and the device parameters. The latter values are difficult to measure or estimate from datasheets as they change with operating conditions and temperature. In this context, there is no obvious way to improve the efficiency of the rectifier without increasing the number of devices, as the line currents are set by the power demand at the dc side and the device parameters cannot be changed or controlled. Two potential solutions are: utilising a higher dc-link voltage [8], which is limited in automotive applications due to the 14 V battery power system and the presence of sensitive loads. Another option is using a multiphase alternator where the same power can be achieved with lower phase currents.

V. High dc-link voltage

The efficiency measurements for the SVM modulation with a higher dc-link voltage are depicted in Fig. 9 [8].

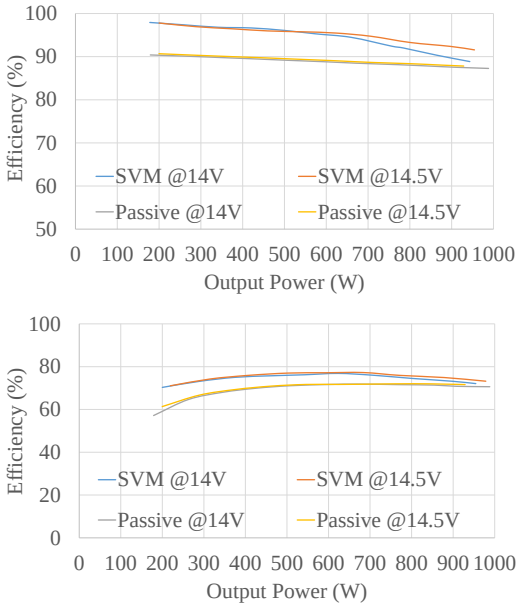

Figure 9: Electrical efficiency (top) and overall efficiency (bottom) at 14.5 V and 2000 rpm

The performance is notably better at high power levels, where the currents are higher. Similarly, Fig. 10 shows the loss breakdown of the active-rectifier. It can be seen that the same power can be achieved with significant lower currents and losses, which in turn allows the operating region of the Lundell alternator/ active-rectifier system to be extended. The efficiency improvement obtained with a 0.5 V higher dc-link voltage is more significant than the one achievable even with an ideal circuitry with no parasitics and is acceptable for a 12 V automotive battery.

VI. Conclusions

This paper has studied in detail the power losses in a Lundell alternator/ active-rectifier system intended for auto-

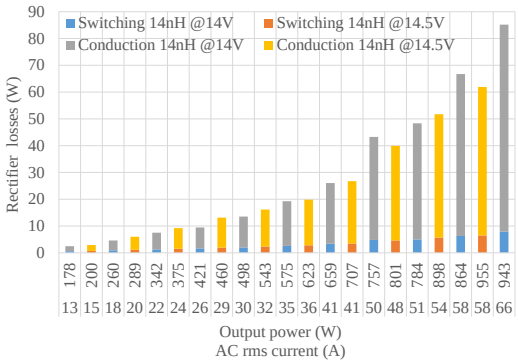

Figure 10: Rectifier breakdown loss comparison

motive applications. Different modulation schemes were tested in an effort to reduce the switching losses. SVM modulation had the best performance as it uses only six commutations per cycle, half of the commutations for a standard PWM modulation, but the overall efficiency was not improved as expected. Then, the double pulse test was simulated to quantify the switching losses in this application using an ideal circuit and also a more realistic scenario with parasitic inductances. Later on, the breakdown of losses in the active-rectifier was carried out with the assistance of the double pulse test results. This breakdown showed that the switching losses have only a marginal share of the total losses, being the conduction losses the most significant component in this application with low dc-link voltage (14 V) and high current. Finally, the dc-link voltage was increased to 14.5 V showing that the same power can be delivered with considerably higher efficiency, allowing the use of a Lundell alternator/ active-rectifier system in a larger range of operation. The authors will extend this control strategy and analysis to a multiphase alternator. Also, a new PCB with lead-less MOSFETs will be designed in an effort to reduce not only the switching losses but also the conduction losses as this package technology has a lower R_{DSon}.

Appendix

References

[1] "Global transport scenarios 2050," World Energy Council, Tech. Rep., 2011.

[2] B. Gmbh, *Automotive eletrics, automotive electronics*, 5th ed., P. R. B. GmbH, Ed. Wiley, 2007.

[3] S. Rees and U. Ammann, "A smart synchronous rectifier for 12 V automobile alternators," in *Power Electronics Specialist Conference, 2003. PESC '03. 2003 IEEE 34th Annual*, vol. 4, June 2003, pp. 1516–1521 vol.4.

[4] T. O'Gorman, D. Stephens, T. Bohn, and R. Carlson, "Automotive Alternator Synchronous Rectificaton Via Self-Sensing Method for Improved Vehicle Fuel Consumption," in *2007 IEEE Industry Applications Annual Meeting*, Sept 2007, pp. 1726–1730.

[5] T. O'Gorman, D. Stephens, B. Conway, and T. Bohn, "A rotor and stator method to increase the power available from an automotive alternator at idle speed," in *2008 Twenty-Third Annual IEEE Applied Power Electronics Conference and Exposition*, Feb 2008, pp. 1991–1998.

[6] F. Liang, J. M. Miller, and X. Xu, "A vehicle electric power generation system with improved output power and efficiency," *IEEE Transactions on Industry Applications*, vol. 35, no. 6, pp. 1341–1346, Nov 1999.

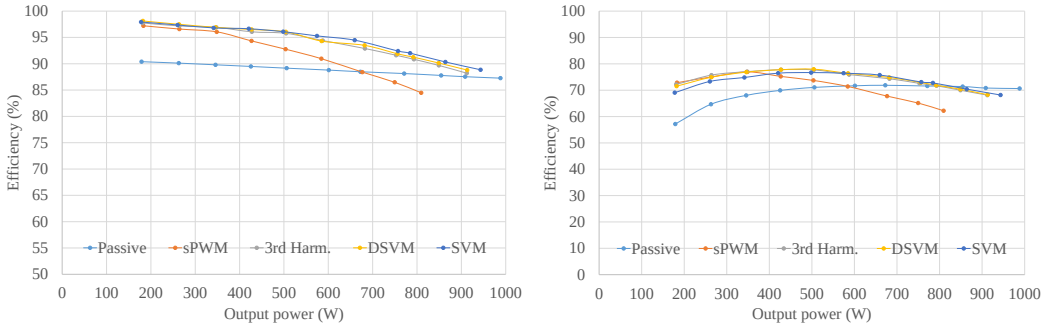

(a) Electrical efficiency (left) and overall efficiency (right) at 2000 rpm

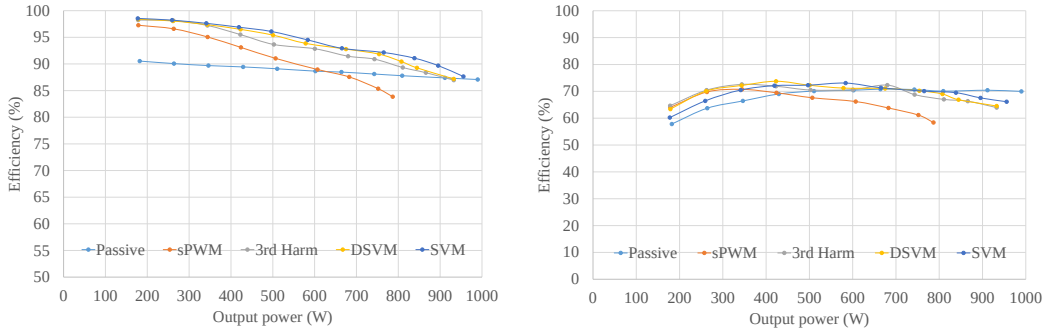

(b) Electrical efficiency (left) and overall efficiency (right) at 3846 rpm

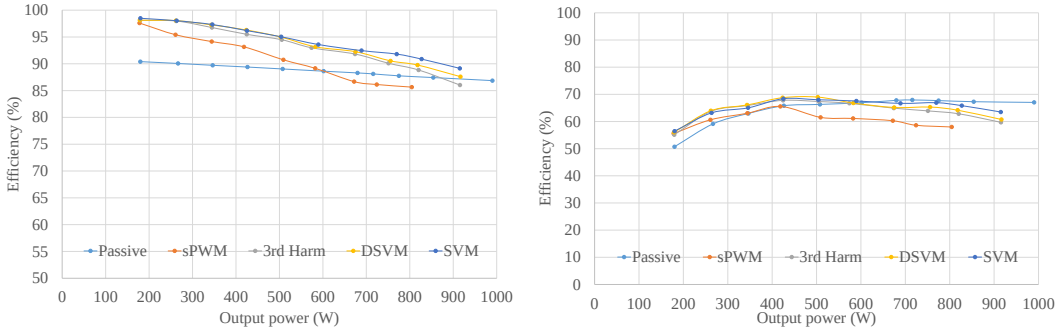

(c) Electrical efficiency (left) and overall efficiency (right) at 5555 rpm

Figure 11: Efficiency measurements

[7] R. Ivankovic, J. Cros, and P. Viarouge, "Experimental comparison of rectifiers for Lundell automotive alternators," in *2009 13th European Conference on Power Electronics and Applications*, Sept 2009, pp. 1–10.

[8] D. Sarafianos, "Lundell alternator modelling and efficiency improvement of conventional vehicle electrical power systems," Ph.D. dissertation, Dept of Engineering, University of Cambridge, 2016.

[9] D. Sarafianos, D. X. Llano, B. Wen, T. J. Flack, R. A. McMahon, and S. Pickering, "Control and efficiency analysis for a Lundell-alternator/active-rectifier system in automotive applications," in *2016 IEEE 2nd Annual Southern Power Electronics Conference (SPEC)*, Dec 2016, pp. 1–6.

[10] S. Safari, A. Castellazzi, and P. Wheeler, "Experimental and Analytical Performance Evaluation of SiC Power Devices in the Matrix Converter," *IEEE Transactions on Power Electronics*, vol. 29, no. 5, pp. 2584–2596, May 2014.

[11] H. Akagi, T. Yamagishi, N. M. L. Tan, S. i. Kinouchi, Y. Miyazaki, and M. Koyama, "Power-Loss Breakdown of a 750-V 100-kW 20-kHz Bidirectional Isolated DC-DC Converter Using SiC-MOSFET/SBD Dual Modules," *IEEE Transactions on Industry Applications*, vol. 51, no. 1, pp. 420–428, Jan 2015.

[12] T. Daranagama, F. Udrea, T. Logan, and R. McMahon, "A performance comparison of SiC and Si devices in a bi-directional converter for distributed energy storage systems," in *2016 IEEE 7th International Symposium on Power Electronics for Distributed Generation Systems (PEDG)*, June 2016, pp. 1–8.

[13] S. Hazra, A. De, S. Bhattacharya, L. Cheng, J. Palmour, M. Schupbach, B. Hull, and S. Allen, "High switching performance of 1.7kV, 50A SiC power MOSFET over Si IGBT for advanced power conversion applications," in *2014 International Power Electronics Conference (IPEC-Hiroshima 2014 - ECCE ASIA)*, May 2014, pp. 3447–3454.

[14] Infineon, "OptiMOS family. The perfect fit for your battery powered application," Tech. Rep., 2014.

[15] D. Graovac, M. Purschel, and A. Kiep., "MOSFET Power Losses Calculation Using the DataSheet Parameters," Tech. Rep., 2006.

[16] Q. Wang, "Investigation and Implementation of MOSFETs Losses Equations in a Three-phase Inverter," Master's thesis, Chalmers University of Technology, 2015.

[17] E. Kahrimanovic, "Power Loss and Optimised MOSFET Selection in BLDC Motor Inverter Designs," Infineon, Tech. Rep., 2016.